JOURNAL OF Materials CHEMISTRY

Hydrothermal synthesis and characterisation of perovskite $BaZn_{1/3}Ta_{2/3}O_3$

Ian MacLaren,*† Shehan Wannakukorale and Clive B. Ponton

IRC in Materials for High Performance Applications and School of Metallurgy and Materials, The University of Birmingham, Birmingham, UK B15 2TT. E-mail: maclaren@fy.chalmers.se

Received 19th April 1999, Accepted 19th July 1999

The hydrothermal synthesis of $BaZn_{1/3}Ta_{2/3}O_3$ has been investigated. Whilst it was relatively straightforward to produce particles having the desired perovskite phase, these particles were deficient in Ba and Zn and correspondingly rich in Ta; some of the excess Zn was precipitated as ZnO. The effects of the metal ion and base concentrations were studied and these were found to affect profoundly the morphology, stoichiometry and crystal structure of the particles. At sufficiently low values of the base concentration, a $BaTa_2O_6$ type phase was produced instead of the perovskite phase. The data from this study were then used to create a stability diagram showing the regions of stability of the perovskite and $BaTa_2O_6$ type phases with respect to the base concentration and the total metal ion concentration.

1 Introduction

There is an increasing market for high-Q microwave resonators for use in the mobile communications industry. In order to produce these as small electronic components for use in hand held communication devices, dielectric ceramics are used which have a reasonable dielectric constant (>20), a low loss at microwave frequencies (often expressed as a high Q factor), and a temperature-stable resonant frequency. One group of materials showing particular promise for this application has the general formula $Ba(X'_{1/3}X''_{2/3})O_3$ (where X′ is Zn, Mg, Ni or other metallic elements which form a divalent ion and X″ is Ta or Nb). Much research has been performed over the last 15–20 years on such materials, particularly concerning $Ba(Zn_{1/3}Ta_{2/3})O_3$ and $Ba(Mg_{1/3}Ta_{2/3})O_3$ based compositions. Whilst higher Q values have been achieved using $Ba(Mg_{1/3}Ta_{2/3})O_3$ based compositions,[1–4] they usually require very high sintering temperatures of *ca.* 1600 °C. By contrast, acceptably good microwave properties can be achieved using $Ba(Zn_{1/3}Ta_{2/3})O_3$ based compositions sintered at lower temperatures of *ca.* 1560 °C.[5–8] This is reflected in the fact that the authors are aware of several industrial companies that produce $Ba(Zn_{1/3}Ta_{2/3})O_3$ based resonators but are not aware of any company producing $Ba(Mg_{1/3}Ta_{2/3})O_3$ on a commercial scale.

Nevertheless, problems are still experienced with the sintering of $Ba(Zn_{1/3}Ta_{2/3})O_3$ owing to the volatility of ZnO at temperatures above 1300 °C resulting in the depletion of ZnO at the surface and the formation of non-perovskite barium tantalate type phases.[9,10] Such non-perovskite phases do not exhibit the same desirable microwave dielectric properties as the perovskite phase and must therefore be eliminated. This can be done either by polishing away the surface after sintering, or by alternative methods such as that of Kawashima where the sample was surrounded with ZnO powder during the sintering process. Unfortunately, this latter method resulted in a reduction of the Q value and it seems that a small Zn deficiency may be required for the achievement of the highest Q values.[10]

An alternative way of minimising the problems associated with ZnO loss at the surface would be to produce a more highly sinteractive powder, so that a higher sintered density could be achieved in a shorter time or at a lower sintering temperature, thus reducing ZnO loss at external surfaces. Chemically synthesised powders often possess fine, narrow particle size distributions and low aspect ratio particle morphologies, as well as good microstructural and chemical homogeneity. These properties tend to result in improved sinterability as compared to conventional mixed oxide route powders. One particularly promising route is that of hydrothermal synthesis, which is the synthesis of ceramic powders from precursor chemicals in aqueous or part-aqueous solution at temperatures above 100 °C and pressures above atmospheric pressure. This route has the advantage over some other chemical synthesis routes that relatively inexpensive salts (such as acetates or nitrates) can be used as metal ion precursors. Additionally, quite a number of compounds can be produced directly in the desired crystalline phase without requiring a calcination step, including barium-based perovskites such as barium titanate[11] and barium magnesium tantalate.[12,13]

This paper reports on some experiments on the hydrothermal synthesis of barium zinc tantalate at temperatures of *ca.* 220 °C. In particular, it is shown that both the metal ion precursor concentration and the base concentration have a critical effect on the phases formed by hydrothermal synthesis, as well as the size, morphology and chemical composition of the resulting particles.

2 Experimental

The raw materials used were barium acetate, $Ba(MeCO_2)_2$, and zinc acetate, $Zn(MeCO_2)_2$, (both from Aldrich Chemical Co., Gillingham, Dorset), and tantalum oxalate solution‡ (H.C. Starck Ltd., Goslar, Germany). The tantalum oxalate was converted to a hydrated tantalum oxide by precipitation with ammonia, and the precipitate washed free of ammonium and oxalate ions as described previously.[12] Starting sols were then produced by dissolving the barium and zinc acetates in deionised water followed by stirring in the hydrated tantalum oxide precipitate. These were then made alkaline using the strong organic base, tetramethylammonium hydroxide (NMe_4OH), (TMAH). Alkaline conditions were used since

†Present address: Department of Physics, Chalmers University of Technology, S-412 96 Göteborg, Sweden.

‡Tantalum oxalate solution does not have a simple chemical formula but the concentration of oxalate ions and tantalum (as Ta_2O_5) in solution is specified by the manufacturers.

the related compound barium magnesium tantalate could only be synthesised in strongly alkaline conditions.

The ideal reaction for the formation of perovskite $BaZn_{1/3}Ta_{2/3}O_3$ (BZT) is given by eqn. (1)

$$3Ba(MeCO_2)_2(aq) + Zn(MeCO_2)_2(aq) + Ta_2O_5 \cdot xH_2O(s) + 8NMe_4{}^+OH^-(aq) \rightarrow 3BaZn_{1/3}Ta_{2/3}O_3(s) + 8(MeCO_2)^-NMe_4{}^+(aq) + (4+x)H_2O \quad (1)$$

Thus, for complete reaction to form perovskite BZT, the ratio of OH^- : total metal ion concentration (assuming complete dissociation of NMe_4OH to $NMe_4{}^+$ and OH^-) should be at least 1.33. Considering the fact that TMAH is known to decompose slowly at temperatures in excess of 150 °C,[12,14,15] the actual molar ratio of TMAH concentration : total metal ion concentration required for formation of perovskite BZT may be somewhat higher than 1.33. Various compositions were produced using different values of the total metal ion concentration in the starting sol (whether fully dissolved or not), M, (from 0.2 to 2 mol l^{-1}) and different ratios of OH^- : total metal ion concentration, B/M, (from 1 to 4) in the starting sol.

The sols were then treated hydrothermally in either of two 250 cm^3 autoclaves (one manufactured by Berghof GMbH, Germany; the other manufactured by Baskerville Reactors and Autoclaves Ltd., Manchester, England) at 220 °C for 2 h with stirring at 500 rpm. The pH values before and after synthesis were recorded to give some idea of the degree of decomposition of the TMAH in the course of the reactions. The hydrothermally processed sols were vacuum filtered and the resultant powder cake washed with water, followed by acetone (to aid drying). The powder cake was dried at room temperature for several days and then powdered using a porcelain pestle and mortar. The powders were then characterised using X-ray diffraction (XRD), transmission electron microscopy (TEM) and FTIR spectroscopy.

XRD was performed using a Phillips X'Pert Diffractometer with Cu-Kα radiation using a 2θ angular range of 10–70°. As for previous work on barium magnesium tantalate,[12] the XRD results were compared against the JCPDS standard 29-203 for $Ba(Zn_{1/3}Ta_{2/3})O_3$ for the purposes of phase identification. It is probable that the samples probably had the disordered cubic perovskite structure rather than the ordered hexagonal structure of well sintered $Ba(Zn_{1/3}Ta_{2/3})O_3$ since the weak superlattice reflections, which are characteristic of the hexagonal structure, were never observed in the XRD traces.

The XRD peaks were typically broadened because the particle size of most of the powders was in the nanometre range. This broadening was used to provide an estimate of the crystallite size from the Scherrer formula [eqn. (2)]:[16]

$$t = 0.9\lambda/B \cos \theta_B \quad (2)$$

where t is the crystallite diameter, λ is the wavelength of the X-rays (1.5418 Å for Cu-Kα), B is the broadening in radians 2θ, and θ_B is the position of the peak maximum in radians. For the perovskite phase, there are four main peaks within the 10–70° 2θ range at *ca.* 30.9, 44.3, 54.8 and 64.3°. The nominal crystallite size was calculated from the average of the results determined from the broadening of each of the four peaks after correcting for the effects of intrinsic peak broadening due to the diffractometer. The degree of intrinsic peak broadening was ascertained from a silicon standard utilising peaks at similar 2θ values to the perovskite peaks, and found to be of much smaller magnitude than the broadening due to size effects. Nevertheless, the size broadening results were corrected for the effects of this intrinsic broadening using the following formula:[16]

$$B^2 = B_M{}^2 - B_S{}^2 \quad (3)$$

where B_M is the measured line breadth for the sample and B_S is the breadth of the line for the standard. Since the broadening due to size effects was so much greater than the intrinsic line broadening due to the diffractometer, the correction to t was usually <1 nm. TEM samples were made by dispersing the powders in methanol, dipping carbon films supported on aluminium grids into the suspension, and removing and then drying the grids on filter paper (thus leaving the BZT particles dispersed on the carbon films). These were then examined using a Phillips CM20 TEM operating at 200 kV which was equipped with a Link AN10000 EDX detector. Use was made of bright field imaging, selected area diffraction and quantitative EDX analysis. Aluminium grids were used in preference to the more usual copper grids since the Cu-K X-ray peaks exhibit significant overlap with the L peaks for Ta and the K peaks for Zn thus making quantification of the BZT stoichiometry problematic. In contrast, the Al-Kα peak has a relatively low energy of 1.486 keV which does not have any overlaps with the main peaks for Ba, Zn or Ta, thus making quantification more straightforward. No attempt was made to quantify the oxygen content from EDX and all compositions are quoted as atomic percent (at.%) of the total metal ion content.

FTIR spectroscopy was performed using a Nicolet Magna-IR 760 spectrometer. Samples were made by mixing 2.5 wt.% of BZT powder with dry spectroscopic grade KBr powder (Fisher Scientific Ltd., Loughborough, Leicestershire) and compacting the mixed powder in a die at a pressure of 200–300 MPa, producing translucent discs. These were then mounted suitably, placed in the main beam of the spectrometer, and the IR absorption in transmission was measured in the range 400–4000 cm^{-1}. A trace was collected by scanning this range 500 times with the sample in place and then removing the sample and collecting a second trace with 500 more scans to determine the background due to the air (including atmospheric CO_2 and H_2O). The background traces were then subtracted from the sample traces to produce the traces shown.

3 Results and discussion

It is relatively straightforward to produce a $Ba(Zn_{1/3}Ta_{2/3})O_3$ powder with the desired perovskite phase. Fig. 1 shows an XRD pattern for one powder produced at the start of this work from a composition with a total metal ion concentration, M, of 1 mol l^{-1} and an OH^- : total metal ions ratio, B/M, of 2. Whilst the main peaks in the XRD trace shown in Fig. 1 are those for the perovskite phase, small peaks may be noted at $2\theta = 31.83$, 34.51 and 36.3°, corresponding to ZnO (hexagonal wurtzite structure, JCPDS 36-1451). The perovskite peaks are somewhat broadened and the particle size of the perovskite particles was estimated to be 19.9 ± 1.7 nm using the Scherrer formula as described above. A TEM micrograph of some particles from this powder is shown in Fig. 2(a) and the SAD pattern of a similar group of particles is inset. The majority of particles are rounded and approximately equiaxed although some irregula-

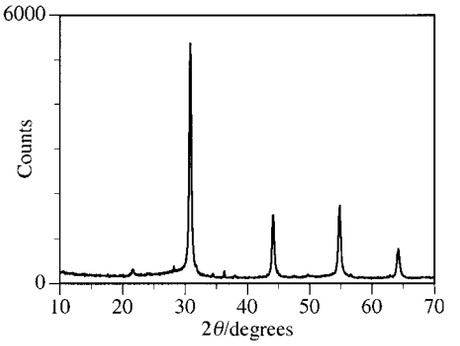

Fig. 1 XRD trace for a $BaZn_{1/3}Ta_{2/3}O_3$ powder produced using $M = 1$ mol l^{-1} and $B/M = 2$.

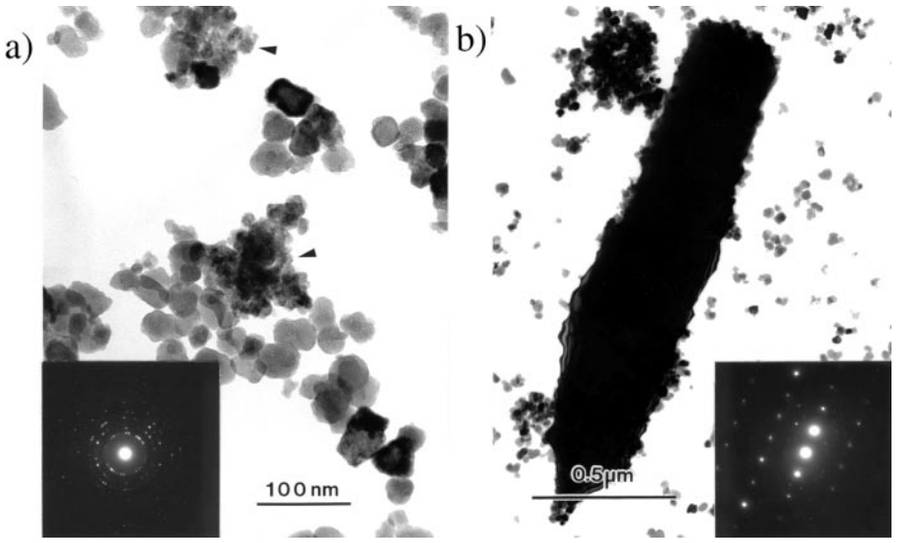

Fig. 2 TEM micrographs of the BZT powder produced using $M = 1$ mol l^{-1} and $B/M = 2$: (a) bright field image of BZT particles with an SAD pattern taken from a similar group of particles inset; (b) ZnO particle (note the lower magnification) with an SAD pattern inset.

rities may be noted. Typical particle dimensions are in the range of 10–40 nm, which agrees well with the size determined from the XRD peak broadening. The ring radii in SAD patterns for these particles are consistent with them being of the perovskite $Ba(Zn_{1/3}Ta_{2/3})O_3$ structure. Quantitative EDX analysis of the larger particles with sizes of *ca.* 20 nm using the TEM showed that they had a composition in the region of 47% Ba, 11% Zn and 42% Ta, that is they are significantly deficient in Zn and slightly deficient in Ba, and correspondingly rich in Ta, as compared with the stoichiometric composition of 50% Ba, 16.7% Zn and 33.3% Ta. The smaller particles are often found in 'fuzzy' clusters, as indicated in Fig. 2(a) with arrows, and have a more Ba and Zn deficient composition of *ca.* 43% Ba, 9% Zn and 48% Ta.

Fig. 2(b) shows a TEM micrograph of a large acicular single crystal of ZnO from this powder (composition from quantitative EDX >99% Zn), as well as some more BZT particles; a SAD pattern taken from the ZnO particle is inset. Most ZnO particles observed in this and in other BZT powders tended to be much larger than the BZT particles, having an acicular morphology (diameters of the order of a few hundred nanometres and lengths of the order of a micron). The SAD pattern corresponds to the [$1\bar{2}10$] zone axis for the hexagonal wurtzite structure of ZnO (as was detected by XRD). The spots which lie parallel to the long axis of the needle arise from the (0002) planes of the crystal structure and thus the long axis of the crystal is parallel to the [0001] axis of the hexagonal structure. Other examples have also been found with the long axis of the crystal parallel to [0001], and hence it seems that these crystals must grow more rapidly in the [0001] direction than in directions perpendicular to it, resulting in the observed acicular morphology of the ZnO crystals.

Thus, whilst it is straightforward to produce the desired perovskite phase, it is seems that, as in the case of the $BaMg_{1/3}Ta_{2/3}O_3$,[12] it is more difficult to achieve the desired stoichiometry and homogeneity. It was decided, therefore, to investigate the effect of the total metal ion precursor concentration and the organic base concentration upon the products in order to understand better the chemistry of this system and hence facilitate the production of a more stoichiometric and homogeneous powder. Firstly, the effect of varying the OH^- : total metal ion ratio (B/M) at a constant metal ion concentration (M) is reported. Then, the effects of varying M at two different values of the B/M ratio are shown.

Table 1 Experimental details for four BZT powders produced to study the effect of varying B/M at a constant value of M; the theoretical yield on 100% conversion to BZT would be 8.19 g

B/M	pH before hydrothermal treatment	pH after hydrothermal treatment	Recovered powder yield/g
1	13.5	10.2	6.96
1.5	13.7	11.1	7.89
2	13.7	11.5	8.51
4	*ca.* 14	*ca.* 11	8.54

3.1 Varying base concentration at a constant metal ion concentration

Four powders were synthesised at $M = 0.5$ mol l^{-1} with values of B/M of 1, 1.5, 2 and 4, respectively. The details for these synthesis runs are shown in Table 1. The recovered yield will include any non-perovskite particles and any residual organic or aqueous species. Fig. 3 shows XRD traces for the four powders produced with values of B/M from 4 to 1. For the three compositions with B/M ratios from 4 down to 1.5, the perovskite phase is formed. Note, however, that the peaks become broader and less intense as the base concentration is reduced. This suggests that the crystallite size is reduced as the B/M ratio is reduced. Estimates of the crystallite size of these particles from the peak broadening give sizes of 21.0 ± 1.9, 8.4 ± 1.4 and 4.3 ± 0.7 nm, for the powders produced with B/M values of 4, 2 and 1.5, respectively. The composition formed at a B/M ratio of 1 displays a quite different XRD trace which

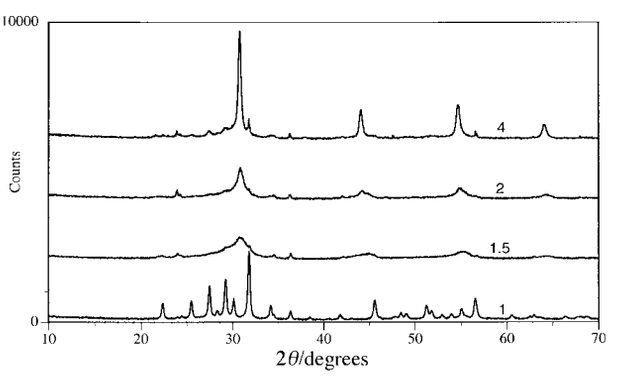

Fig. 3 XRD traces for BZT powders produced at $M = 0.5$ mol l^{-1} with $B/M = 4$, 2, 1.5 and 1, respectively.

matches with one of the tungsten bronze type $BaTa_2O_6$ phases (JCPDS 17-0793). It seems, therefore, that as the B/M ratio is reduced, the resulting perovskite phase becomes less well crystallised until, at some ratio between 1.5 and 1, a $BaTa_2O_6$ type phase is formed instead.

Fig. 4(a)–(d) show TEM micrographs of the four powders. The powder formed at $B/M=4$ [Fig. 4(a)] had some larger rounded particles (marked **1**), as well as 'fuzzy' clusters of smaller rounded or irregular shaped particles (marked **2**), and a few particles with needle-like or thin rectangular platelet morphologies (marked **3**). EDX gave compositions for the rounded particles of *ca.* 48% Ba, 12% Zn and 40% Ta, and compositions for the 'fuzzy' clusters of 41% Ba, 9% Zn and 50% Ta. Analysis of SAD patterns showed that both of these types of particles were of the perovskite BZT phase. The needles had a totally different composition of *ca.* 38% Ba, 1% Zn and 61% Ta and were believed to be of the $BaTa_2O_6$ phase.

The powder formed at $B/M=2$ was qualitatively similar [Fig. 4(b)] to that formed at $B/M=4$, although there was a lower proportion of larger rounded particles and a higher proportion of the 'fuzzy' clusters. The compositions from EDX were similar to those for the $B/M=4$ powder but there was less of a clear distinction between the compositions for the rounded particles and the fuzzy clusters, and an average composition of 46% Ba, 8% Zn and 46% Ta was found for all these particles. As in the case of the $B/M=4$ powder, analysis of SAD patterns showed that these particles were of the perovskite BZT phase. The compositions of the small needles were *ca.* 37% Ba, 6% Zn and 57% Ta, and these were thought to be of the $BaTa_2O_6$ phase, as for the $B/M=4$ powder.

The powder formed at $B/M=1.5$ [Fig. 4(c)] did not contain any of the rounded perovskite particles but only small 'fuzzy' clusters of ultrafine irregular particles, and needle shaped particles. The 'fuzzy' clusters had compositions of *ca.* 43% Ba, 5% Zn and 52% Ta, which is more Ta-rich and Zn-deficient than in the $B/M=4$ or 2 powders. As for those two powders, analysis of SAD patterns showed that these particles were of the perovskite BZT phase although the spots were less well defined as a consequence of the ultrafine particle dimensions. The needle shaped $BaTa_2O_6$ particles had compositions of *ca.* 34% Ba, 6% Zn and 60% Ta.

The powder formed at $B/M=1$ [Fig. 4(d)] was somewhat different to the others in that no perovskite BZT particles were observed and it consisted mostly of rectangular platelet or needle shaped particles with similar morphologies to the $BaTa_2O_6$ particles observed in the other powders. All of these particles had similar compositions, with the average composition being *ca.* 36% Ba, 6% Zn and 58% Ta.

All of the four powders were found by TEM/EDX to contain large single crystal ZnO needles with metal ion contents of $>99\%$ Zn, most of which had diameters of a few hundred nanometres and lengths of the order of 1 micron. The $B/M=4$ powder was an exception, however, in that the few needles observed were much longer by comparison (8 μm in one case) but had a similar diameter to the needles observed in the other powders. The reasons for this are not totally clear although it

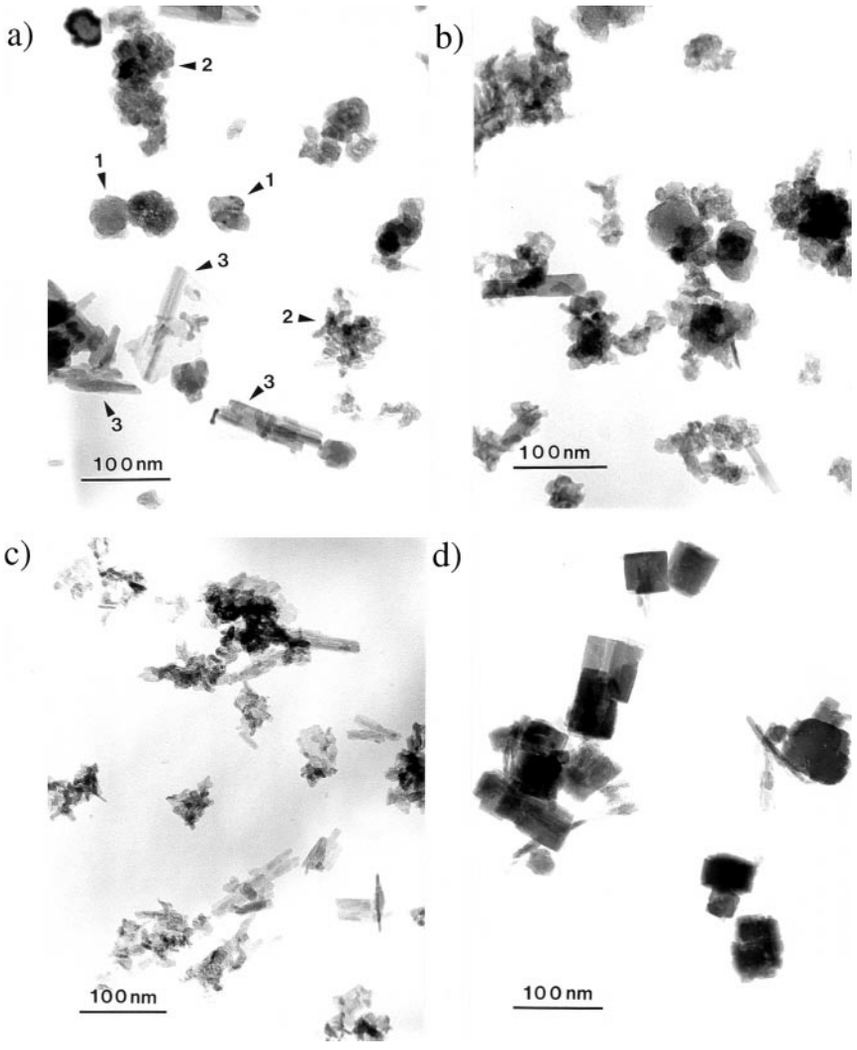

Fig. 4 TEM micrographs of BZT powders produced at $M=0.5\ mol\ l^{-1}$: (a) $B/M=4$; (b) $B/M=2$; (c) $B/M=1.5$ and (d) $B/M=1$.

would appear that the conditions for the growth of large ZnO needles were extremely good in these very alkaline conditions. Since Zn is an amphoteric metal, its solubility would be high at the start of these reactions but would fall both during the reaction because of the pH reduction (owing to the loss of free OH^- ions in the solution due to participation in the reaction as outlined in eqn. (1), and the increasing decomposition of TMAH on heating to 220 °C and during the course of the reaction at 220 °C), and on cooling from the 220 °C reaction temperature back to room temperature.

Fig. 5 shows FTIR traces for these four powders. The broad hump centred around 3400 cm^{-1} probably arises from water and hydroxy groups adsorbed onto and incorporated into the BZT particles. The small peaks at *ca.* 2920 and 2850 cm^{-1} are thought to arise from C–H stretching vibrations of CH, CH_2 or CH_3 groups in molecules adsorbed on the particle surfaces. The noisy peaks in the region of 2330–2380 cm^{-1} arise from absorption peaks for atmospheric CO_2 which have not been removed completely by the background subtraction. The small peak in the traces for $B/M=4$, 2 and 1.5 at 1748 or 1749 cm^{-1} was considered to arise from the C=O bond in any acetate species which are adsorbed onto the surfaces of the particles. The peak at 1615–1625 cm^{-1} was believed to be a vibration of water, either adsorbed on the particle surfaces or incorporated into the crystal lattice. These are all the peaks that could be assigned confidently to organic or aqueous species. It can be seen, therefore, that all the powders contained a certain amount of adsorbed/incorporated water and perhaps hydroxy ions, as well as a small amount of adsorbed acetate (identified from the C=O and C–H vibrations). It is clear, however, that the amount of water adsorbed onto or incorporated into the particles during the synthesis reaction reduces with increasing base strength.

The origin of the large peak at 1423 or 1436 cm^{-1} was uncertain as it could not be assigned to any organic or aqueous species, although it may be associated with vibrations of the perovskite structure. The only FTIR study of perovskite $Ba(Zn_{1/3}Ta_{2/3})O_3$ that we are aware of,[7] however, just reports the vibrations for sintered ceramic samples that had the ordered hexagonal structure, and not the vibrations for particulate samples with the disordered cubic structure, as in this study. No peak around 1420–1440 cm^{-1} is reported in that study. The small broad peak at around 1000–1020 cm^{-1} could possibly arise from Ta–O vibrations.[18,19] Similarly, the sharp peak at around 856 cm^{-1} may have arisen from Ta–O vibrations since

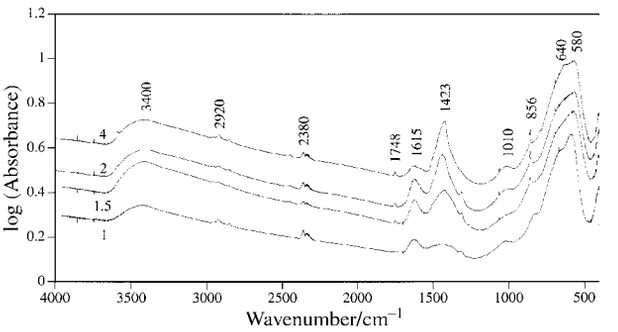

Fig. 5 FTIR traces for BZT powders produced at $M=0.5$ mol l^{-1} with $B/M=4$, 2, 1.5 and 1, respectively, in the range 400–4000 cm^{-1}.

there are a number of vibrations recorded for Ta–O in the region of[19] 880–940 cm^{-1} and the frequency of the vibration could have been reduced by the effect of the crystalline lattice. The final and largest peak is somewhat broadened with a shoulder at around 640–660 cm^{-1} and the main peak at 580–581 cm^{-1}. Thomas and Andrews[20] found that the Ba–O bond vibrates at about 635 cm^{-1} and it may be that this large peak is substantially the result of Ba–O vibrations. This peak does not vary greatly from one powder to another and so the coordination of the barium ions in the BZT powder (if it really does relate to the Ba–O vibrations) is not affected greatly by the B/M ratio employed in the synthesis reaction. According to Prochaska and Andrews,[21] the Zn–O bond vibrates at 802 cm^{-1}. No peak was found which corresponds unequivocally to this vibration, unless it was the slight bump at 797 cm^{-1} on the edge of the large Ba–O peak for the trace for $B/M=4$.

In summary, these lower wavenumber infrared absorption peaks are difficult to characterise for these BZT samples and there are certain to be effects of the vibration of the whole crystal structure upon these peaks, and not just of the individual metal–oxygen bond vibrations. For this reason, the peak assignments in the range 400–1500 cm^{-1} should be regarded as tentative and more detailed work on the FTIR characterisation of $Ba(Zn,Ta)O_3$ powders would be very useful in establishing definitively the origin of the peaks in this region of the IR spectrum.

3.2 Varying the metal ion concentration at a constant ratio of base : metal ions

A number of runs were performed with B/M ratios of 1 and 2 at different metal ion concentrations. Firstly, the results for $B/M=1$ are presented, followed by those for $B/M=2$.

3.2.1 ***B/M*=1.** Six powders were produced at various M values from 0.2 to 2 mol l^{-1} in order to study the effect of M on powders produced at $B/M=1$; details of these synthesis runs are given in Table 2. As before, the recovered yield will include non-perovskite particles and any residual organic or aqueous species.

Fig. 6 shows the XRD traces for these samples. The peak positions for all these samples match to a $BaTa_2O_6$ type phase (JCPDS 17-0793) with no peaks for the perovskite phase. Whilst there is some intensity variation from one trace to another, the width of these peaks is similar for most of these traces suggesting that there is little difference in crystallite size between most of these particles. Since our TEM observations of $BaTa_2O_6$-type particles invariably show them as thin platelets or needle-like in morphology, the apparent particle dimensions from Scherrer broadening of the XRD peaks will vary widely from one reflection to another depending on how the set of planes giving rise to the reflection are oriented with respect to the crystallite morphology. Thus, no accurate estimate of the crystallite size could be made from Scherrer broadening of the XRD peaks, apart from saying that the particle dimensions are of the order of tens of nanometres.

TEM studies show that the particle size, morphology and stoichiometry observed for the various powders produced at $B/M=1$ are fairly similar to those for the particles shown in Fig. 4(d) (from the powder produced at $M=0.5$ mol l^{-1}).

Table 2 Experimental details for six BZT powders produced to study the effect of M at $B/M=1$

M/mol l^{-1}	pH before synthesis	pH after synthesis	Recovered powder yield/g	Theoretical yield for perovskite BZT/g
0.2	12.8	10.5	2.68	3.28
0.5	13.3	11.5	7.27	8.19
0.6	13.2	11.1	8.88	9.83
0.8	13.4	11.2	8.85	13.11
1.0	13.4	10.2	22.69	16.39
2.0	14.4	11.0	34.93	32.78

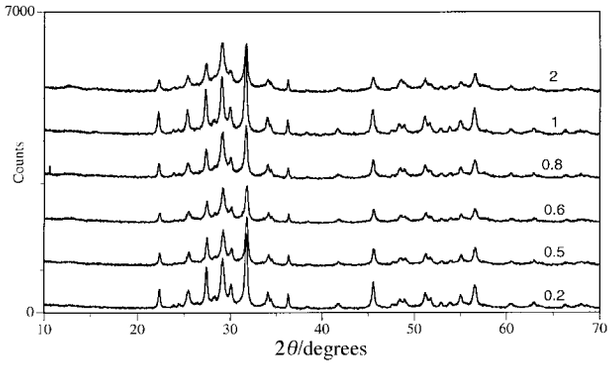

Fig. 6 XRD traces for BZT powders produced at $B/M=1$ with values of M in the range 0.2–2 mol l^{-1}.

Another example is shown in Fig. 7; this is a TEM image of particles in the powder produced at $M=1$ mol l^{-1}. As can be seen from these two figures, most of the particles in these powders are thin rectangular platelets or small needle shaped particles. These were found by EDX to have metal ion compositions in the range of 55–65% Ta, 30–35% Ba and 4–10% Zn. Large ZnO needles (with metal ion compositions of >99% Zn) were also observed in these powders.

In conclusion, at $B/M=1$, the $BaTa_2O_6$ type phase is formed over a range of metal ion concentrations from 0.2 to 2 mol l^{-1}. No evidence for the formation of a perovskite phase was found in any of these samples, suggesting that this B/M ratio is insufficient to cause even the formation of some highly Zn and Ba deficient perovskite particles. TEM observations show that the $BaTa_2O_6$ type phase is non-stoichiometric with typically less Ta than required for stoichiometry and some substitution of Zn for Ta and Ba. It may also be noted from both the TEM and XRD results that neither the crystallinity, nor the particle size and morphology are affected to any significant extent by the metal ion concentration.

3.2.2 ***B/M*=2.** Three powders were produced at different values of M from 0.2 to 1 mol l^{-1} to study the effect of M on the resulting powders at $B/M=2$; the details of these synthesis runs are given in Table 3. Two of these powders have already been referred to in previous sections (those produced at $M=1$ and 0.5 mol l^{-1}) but the results are discussed here also with regard to the effect of M on the powders with $B/M=2$.

Fig. 8 shows the XRD traces for these three powders. It can be seen clearly that the peaks become lower in intensity and broader as M is reduced suggesting that both the degree of crystallinity and the crystallite size of the powders decrease as M is reduced. Indeed, Scherrer X-ray line broadening estimates of the crystallite size for the three powders give values of 19.9 ± 1.7, 8.4 ± 1.4 and 5.4 ± 0.5 nm for the powders produced at $M=1$, 0.5 and 0.2 mol l^{-1}, respectively.

Images of the particles produced at $M=1$ and 0.5 mol l^{-1} have already been shown in Fig. 2(a) and 4(b), respectively. Fig. 9 shows a TEM image of the powder produced at $M=0.2$ mol l^{-1}. As with other samples which show significant XRD peak broadening, the particles are small clusters of ultrafine irregular crystallites, some of which are somewhat elongated in morphology. The compositions of these particles were determined by EDX and an average of the analyses of five particles gave a result of 44 ± 1% Ba, 5 ± 0.5% Zn and 51 ± 1% Ta. Some needle-shaped $BaTa_2O_6$ particles were also noted, as were large ZnO needles.

Fig. 7 TEM image of a BZT powder produced with $B/M=1$ and $M=1$ mol l^{-1}.

In summary, for $B/M=2$ and the range of M values that we have investigated, perovskite phase BZT particles are always formed as the predominant phase, although particles with the $BaTa_2O_6$ structure and ZnO particles are also present in the powders. In contrast to the powders produced using $B/M=1$, the size, morphology and stoichiometry of the powders are all strongly dependent on the metal ion concentration, M. That is, perovskite particles produced at high values of M tended to be more rounded and near stoichiometric, while those produced at lower values of M tended to form as small clusters of ultrafine irregular crystallites having smallest cross sectional diameters of the order of 5 nm.

3.3 Stability diagram for BZT synthesis

Lencka and Riman have used a thermodynamic approach to predict the regions of stability of phases in hydrothermal conditions at given temperatures and pressures with respect to the concentration of the solution and the pH.[22,23] They have

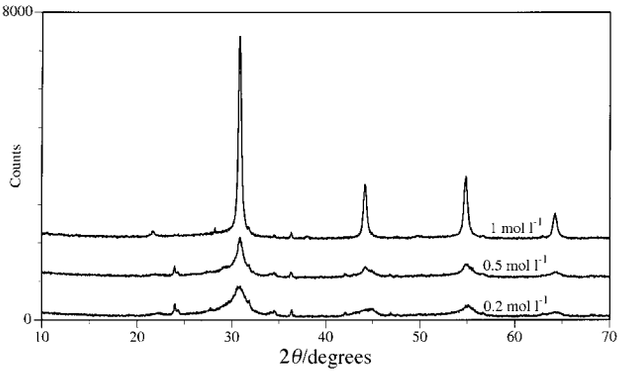

Fig. 8 XRD traces for BZT powders produced at $B/M=2$ with values of M in the range 0.2–1 mol l^{-1}.

Table 3 Experimental details for three BZT powders produced in order to study the effect of varying M at $B/M=2$

M/mol l^{-1}	pH before synthesis	pH after synthesis	Recovered powder yield/g	Theoretical yield for perovskite BZT/g
0.2	13.3	12.1	3.26	3.28
0.5	13.7	11.5	8.51	8.19
1.0	14.2	11.0	16.10	16.39

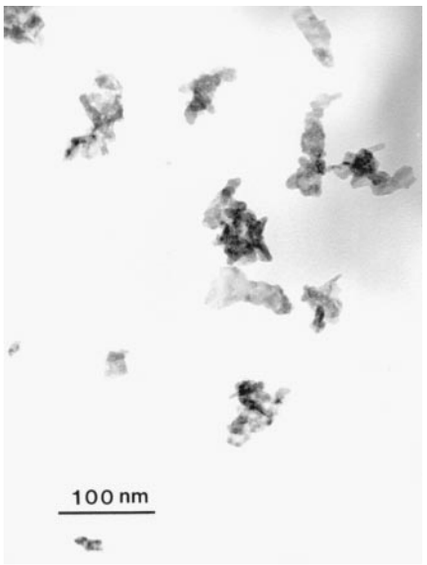

Fig. 9 TEM image of a BZT powder produced with $B/M=2$ and $M=0.2$ mol l^{-1}.

then verified these predictions using selected hydrothermal experiments. At present, however, they have only worked on perovskite titanates and zirconates. It is not currently possible to devise similar thermodynamic models for tantalate systems owing to insufficient reliable thermodynamic data for tantalum in solution.[24] It is to be hoped, however, that workers with an interest in hydrothermal chemistry will take up the challenge of making the relevant measurements. In the meantime, the data presented in this paper may give some indications about the regions of phase stability for this system under hydrothermal conditions.

Most experiments conducted by Riman's group employed inorganic bases such as barium hydroxide, ammonia solution or potassium hydroxide.[22,23,25] These do not decompose during the reaction so that the pH at the end of the reaction is effectively the equilibrium pH which can be plotted readily on a stability diagram. In the reactions reported in this paper, however, we have used a strong organic base to avoid the contamination of the product by sodium or potassium ions, as in our previous work.[12,13] This base begins to decompose at temperatures above 150 °C resulting in there being two modes of pH reduction: namely elimination of OH^- ions in the formation of the BZT phase, as shown in the chemical eqn. (1), and decomposition of the TMAH to trimethylamine and methanol [eqn. (4)][26] [trimethylamine is a weak base and behaves in solution in a similar way to ammonia, eqn. (5)].

$$NMe_4{}^+OH^-(aq) \Rightarrow NMe_3(aq) + MeOH(l) \quad (4)$$

$$NMe_3(aq) + H_2O(l) \Leftrightarrow NHMe_3{}^+(aq) + OH^-(aq) \quad (5)$$

The latter process had a very strong effect on the final solution pH and, hence, the room temperature pH of the hydrothermally processed sols did not always correlate clearly with the phases formed, whereas there was always a strong correlation with the initial B/M ratio. It would, therefore, if possible, be better to employ an organic base that does not decompose significantly at 220 °C, or be able to work at a lower temperature where the decomposition of TMAH is rather slower. Unfortunately, experiments so far have shown that, while the perovskite phase may be formed at lower temperatures (syntheses at 120 and 170 °C also gave perovskite BZT), the crystallinity is much lower and the particle size is much smaller, with only highly Zn and Ba deficient perovskite particles being formed.

In view of these problems with variable pH values, it was decided to plot reactant concentration against base concentration. Since Riman's group[22,23,25] has generally used the molality of one of the reactants as a measure of reactant concentration, we have converted the concentrations to the molality of barium, m_{Ba}. Similarly, the concentration of base is represented as the molality of TMAH, m_{TMAH}. The conversions of molarity to molality are somewhat approximate since the weight of hydrated Ta oxide varied a little from one batch to another (± 1.5 g) as the degree of drying during filtration is somewhat difficult to reproduce (*i.e.* the water content of the hydrated Ta oxide was a little variable but this did not affect the Ta content). Fig. 10 is a plot of m_{Ba} *vs.* m_{TMAH} with the regions for the formation of the $BaTa_2O_6$ and the perovskite BZT phases demarcated.

This diagram differs in another important manner from the stability and yield diagrams of Riman and coworkers:[22,23,25] in those diagrams it is assumed that the desired phase is formed in a stoichiometric composition. In this case, however, none of the points represented on the diagram for the perovskite phase correspond to fully stoichiometric BZT. Moreover, the composition is somewhat variable and the Zn deficiency increases close to the boundary with the field for the formation of the $BaTa_2O_6$ phase, and at lower Ba concentrations.

At this point in time, no way has been found to produce fully stoichiometric perovskite BZT, and it is not clear if it is possible from just the precursors used in this paper. It is evident, however, that increasing both the precursor concentration and the B/M ratio improves the stoichiometry of the powder particles. This probably occurs since the solution will be more saturated at higher reactant concentrations (*i.e.* metal ion and base concentrations) facilitating the reaction of the Zn ions with the other metal ions hence the precipitation of BZT producing BZT particles that are more stoichiometric. It is not clear, however, how much advantage could be gained by further increasing the precursor concentration. Practically, it would require the use of TMAH in powdered form to obtain a sufficiently high base concentration.

Increasing the B/M ratio is only useful up to a point as was demonstrated by the powder produced at $B/M=4$, where there was an increase in the amount of ZnO produced. The difficulty in producing stoichiometric BZT is probably related to the amphoteric nature of Zn. At the high base concentrations required for producing a highly crystalline perovskite powder, the Zn ions will be reasonably soluble (as zincate complexes) and so a certain proportion will remain in solution rather than react with the other metal ions and coprecipitate BZT. Since, however, the pH is reduced as the TMAH decomposes, the Zn will become less soluble and will precipitate out as ZnO both during the reaction and as the temperature is reduced after

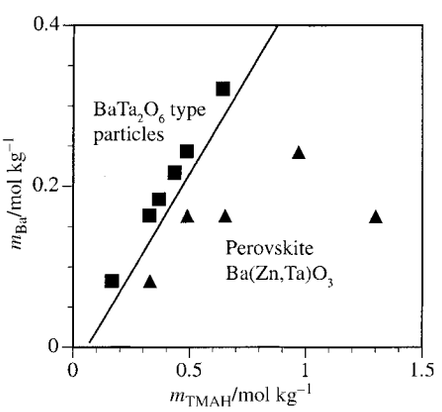

Fig. 10 An experimental stability diagram for the BZT system with barium molality, m_{Ba}, plotted *vs.* TMAH molality, m_{TMAH}. ▲; symbols indicate points at which the perovskite phase was formed and ■ symbols indicate points at which the $BaTa_2O_6$ type phase was formed. The line shows the approximate boundary between the stability regimes for these two phases.

synthesis. Thus, in order to form a stoichiometric BZT powder, a way must be found to change the chemistry of the system to encourage the Zn to react more fully and coprecipitate more, perhaps by reducing the solubility of the Zn throughout the reaction. It may be that a change of solvent system would help to modify the reaction conditions so that fuller Zn coprecipitation could be achieved, resulting in a stoichiometric BZT powder, as in the manner demonstrated previously for $BaMg_{1/3}Ta_{2/3}O_3$.[12,13]

It may be noted that the existence of a clear link between morphology and stoichiometry of the perovskite particles shown in sections 3.1 and 3.2 has been observed previously in the hydrothermal synthesis of the related compound, $BaMg_{1/3}Ta_{2/3}O_3$.[12,13] It was found in that study, also, that particles closer to stoichiometry tend to have rounded morphologies whereas more Ta rich particles tend to form as clusters of ultrafine, irregular crystallites.

This suggests that there may be some factors common to the synthesis of both these materials which have yet to be elucidated. For this reason, it is thought that further study of both these systems, particularly with the aid of thermodynamic modelling of the hydrothermal reactions, may help in understanding better the processes occurring in the formation of either stoichiometric or non-stoichiometric particles and thus aid in the development of a methodology for the production of stoichiometric, homogeneous powders.

4 Conclusions

It has been shown that perovskite phase $Ba(Zn,Ta)O_3$ can be produced readily by hydrothermal synthesis, provided the starting sol is sufficiently alkaline (*i.e.* with a OH^- : metal ion ratio of at least 1.5). There is a tendency, however for all the perovskite particles to be deficient in Ba and Zn and correspondingly rich in Ta. This deficiency is increased as the OH^- : metal ion ratio is reduced towards 1.5. At a lower ratio of 1, the perovskite phase is not formed at all and a $BaTa_2O_6$ type phase is produced instead. In all cases, some of the remaining Zn is precipitated out as large ZnO needles.

It was shown that the morphology of perovskite particles correlates strongly with composition. Thus, those nearest to stoichiometry exhibited rounded morphologies and larger dimensions of the order of 20 nm, whereas the more Ba and Zn deficient particles consisted of clusters of ultra-fine (5–10 nm) irregular crystallites. FTIR analysis showed that the particles produced at the highest base strengths possessed the smallest amount of lattice-incorporated/surface-adsorbed water and that this increased as the base strength was reduced.

It was found that powders comprising mainly particles with the $BaTa_2O_6$ phase were not affected significantly by changes in total metal ion concentration (at a constant OH^- : metal ion ratio). This was in strong contrast to the perovskite powders, the particles of which became more irregular as well as more Ba and Zn deficient as the total metal ion concentration was reduced.

Finally, the data from the different experiments were combined to form a tentative diagram of the stability regions for the perovskite and $BaTa_2O_6$ phases with regard to the initial molar concentrations of the Ba^{2+} ions and the organic base.

5 Acknowledgements

The authors would like to thank Prof. M. H. Loretto (Director of the IRC in Materials for High Performance Applications) and Prof. I. R. Harris (Head of the School of Metallurgy and Materials) for the provision of laboratory facilities. We would also like to thank Mr F. Biddlestone for assistance with the use of the FTIR spectrometer and Dr J. Hay for assistance with the interpretation of FTIR spectra. Part of this work was supported by the Engineering and Physical Sciences Research Council in the UK.

References

1 K. Matsumoto, T. Hiuga, K. Takada and H. Ichimura, *IEEE Trans. UFFC*, 1986, **33**, 802.
2 H. Matsumoto, H. Tamura and K. Wakino, *Jpn. J. Appl. Phys.*, 1991, **30**, 2347.
3 X. M. Chen, Y. Suzuki and N. Sato, *J. Mater. Sci. Mater. Electron.*, 1994, **5**, 244.
4 M. Furuya and A. Ochi, *Jpn. J. Appl. Phys.*, 1994, **33**, 5482.
5 S. Kawashima, M. Nishida, I. Ueda and H. Ouchi, *J. Am. Ceram. Soc.*, 1983, **66**, 421.
6 H. Tamura, T. Konoike, Y. Sakabe and K. Wakino, *J. Am. Ceram. Soc.*, 1984, **67**, C59.
7 Z. L. Zhao, S. L. Lai and A. S. Liu, *Electron. Lett.*, 1990, **26**, 1605.
8 K. Kageyama, *J. Am. Ceram. Soc.*, 1992, **75**, 1767.
9 S. B. Desu and H. M. O'Bryan, *J. Am. Ceram. Soc.*, 1985, **68**, 546.
10 S. Kawashima, *Am. Ceram. Soc. Bull.*, 1993, **72**, 120.
11 R. Vivekanandan, S. Philip and T. R. N. Kutty, *Mater. Res. Bull.*, 1986, **22**, 99.
12 I. MacLaren and C. B. Ponton, *J. Mater. Sci.*, 1998, **33**, 17.
13 I. MacLaren and C. B. Ponton, *Electron Microscopy and Analysis 1997*, ed. J. M. Rodenburg, Institute of Physics Conference Series, IOP Publishing, Bristol, UK, 1997, vol. 153, p. 531.
14 *The Merck Index: an Encyclopedia of Chemicals, Drugs and Biologicals*, Merck, Rahway, NJ, 11th edn., 1989, ref. 9155.
15 D. Hennings, G. Rosenstein and H. Schreinemacher, *J. Eur. Ceram. Soc.*, 1991, **8**, 107.
16 B. D. Cullity, *Elements of X-Ray Diffraction*, Addison-Wesley, Reading, MA, 1978, p. 284.
17 H. Tamura, D. A. Sagala and K. Wakino, *Jpn. J. Appl. Phys., Part 1*, 1986, **25**, 787.
18 K. Nakamoto, *Infrared and Raman Spectra of Inorganic and Coordination Compounds*, Wiley, New York, 1986, p. 106.
19 W. Weltner Jr. and D. McLeod Jr., *J. Chem. Phys.*, 1965, **42**, 882.
20 D. M. Thomas and L. Andrews, *J. Mol. Spectrosc.*, 1974, **50**, 220.
21 E. S. Prochaska and L. Andrews, *J. Chem. Phys.*, 1980, **72**, 6782.
22 M. M. Lencka and R. E. Riman, *Chem. Mater.*, 1993, **5**, 61.
23 M. M. Lencka and R. E. Riman, *J. Am. Ceram. Soc.*, 1993, **76**, 2649.
24 R. E. Riman, personal communication, 1997.
25 M. M. Lencka, A. Anderko and R. E. Riman, *J. Am. Ceram. Soc.*, 1995, **78**, 2609.
26 A. Streitwieser, C. H. Heathcock and E. M. Kosower, *Introduction to Organic Chemistry*, Macmillan, New York, NY, 4th edn., 1992, p. 762.

Paper 9/03080H